PCCP

ROYAL SOCIETY OF CHEMISTRY

PAPER

View Article Online
View Journal | View Issue

Check for updates

Cite this: *Phys. Chem. Chem. Phys.*, 2025, **27**, 11017

Mixed functionalization as a pathway to induce superconductivity in MXenes: vanadium and niobium carbide†

Prarena Jamwal,[a] Rajeev Ahuja [ab] and Rakesh Kumar *[a]

The functionalization versatility of MXenes distinguishes them from other two-dimensional materials, enabling the design of numerous new materials with unique properties. By leveraging surface chemistry, functionalization allows for the manipulation of critical parameters such as the density of states and electron–phonon coupling, providing an excellent platform for exploring two-dimensional superconductivity. In this study, we investigate the impact of functionalization on vanadium carbide (V_2C) MXene, which is intrinsically non-superconducting, by considering three different cases: (i) hydrogen adatoms, (ii) fluorine adatoms, and (iii) mixed functionalization with hydrogen and fluorine adatoms. We confirm the mechanical and dynamical stability of functionalized V_2C using Born's stability criteria and phonon dispersion analyses. In all three cases, superconductivity emerges due to the presence of functional groups, which influence the electron–phonon interaction and electronic structure, leading to an enhanced electron–phonon coupling constant. The highest superconducting transition temperature is observed for mixed-functionalized V_2C, attributed to the softening of the ZA phonon mode along with high-energy phonon modes induced by hydrogen. To further explore the potential of mixed functionalization in inducing superconductivity, we extend our approach to another non-superconducting MXene, Nb_2C. The mixed-functionalized Nb_2C exhibits a superconducting transition temperature of 9.2 K, which surpasses the reported values for Nb_2CH_2, Nb_2CS_2, and Nb_2CBr_2. These findings underscore the effectiveness of mixed functionalization in enabling superconductivity in MXenes, paving the way for future theoretical and experimental investigations.

Received 27th February 2025,
Accepted 25th April 2025

DOI: 10.1039/d5cp00774g

rsc.li/pccp

Open Access Article. Published on 25 April 2025. Downloaded on 2/15/2026 1:18:58 AM.
This article is licensed under a Creative Commons Attribution-NonCommercial 3.0 Unported Licence.

1. Introduction

The dynasty of two-dimensional (2D) materials expanded by the inclusion of 2D layers of transition metal – carbides, nitrides, and carbonitrides, collectively known as MXenes.[1,2] They exhibit variable surface chemistry and a wide range of electronic properties, making them promising candidates for ion batteries,[3] supercapacitors,[4] catalysis,[5] sensing,[6] thermoelectric materials,[7] biomedicine,[8] and energy storage devices.[9] MXenes are typically synthesized from the corresponding MAX phases, where M stands for the transition metal and X stands for carbon or nitrogen, by selectively etching the element A (*e.g.*, Al, Ga, Si, *etc.*) using hydrofluoric acid, molten inorganic salts, a mixture of fluoride salts and various acids.[10–12] The etching results in 2D MX layers terminated with multiple functional groups, which reduce their chemical potential and increase their thermodynamic stability.[13] The random distribution of terminal groups has been verified in various transition-metal carbides using electron-energy loss spectroscopy in transmission electron microscopy,[14] nuclear magnetic resonance spectroscopy,[15] and X-ray photoelectron spectroscopy.[16] The presence of single or mixed terminations in MXenes depends on their synthesis or processing conditions.[12,17] This capability to modify surface terminations enhances their extensive compositional diversity, setting them apart from other 2D materials.

Most of the MXenes exhibit metallic behavior, reflected from their electronic structure calculations, and tuning their electronic properties by surface functionalization makes them possible candidates for hosting superconductivity in the 2D limit.[18] Some recent experimental and theoretical studies highlight the significance of surface terminations in inducing and enhancing superconductivity, leveraging the unsaturated surface chemistry of MXenes. Researchers are actively investigating the possible ways of surface functionalization of MXenes to explore superconductivity. For instance, pristine Nb_2C has been reported as a non-superconducting material in experimental

[a] *Department of Physics, Indian Institute of Technology Ropar, Punjab-140001, India*
[b] *Condensed Matter Theory Group, Department of Physics and Astronomy, Uppsala University, Box 516, Uppsala-75120, Sweden. E-mail: rakesh@iitrpr.ac.in*

† Electronic supplementary information (ESI) available. See DOI: https://doi.org/10.1039/d5cp00774g

Open Access Article. Published on 25 April 2025. Downloaded on 2/15/2026 1:18:58 AM. This article is licensed under a Creative Commons Attribution-NonCommercial 3.0 Unported Licence.

and theoretical studies.[19,20] However, theoretical investigations have revealed the emergence of superconductivity in Nb_2C through Cl adatoms, achieving a superconducting transition temperature (T_c) of approximately 6 K, which is further increased to 37.8 K with charge carrier doping.[21] The experimental studies also report the induction of superconductivity in Nb_2C under surface functionalization.[19,22] Recent experimental reports have shown the feasibility of controlled surface functionalization of MXenes. For instance, Xia *et al.* synthesized fluorine-functionalized Mo_2C by sintering a mixture of Mo_2C and NH_4F, observing an enhanced T_c of 5.7 K compared to the 3.2 K of pure Mo_2C.[17] Similarly, prior theoretical studies have demonstrated enhanced superconductivity in Mo_2C through surface functionalization, with T_c values reaching up to 13 K for Br[23] and H[24] adatoms. In the nitride counterparts, such as Mo_2N and W_2N, hydrogenation significantly increases T_c from 16 K to 32.4 K and 10 K to 30.7 K, respectively.[24] Further studies are needed to better understand the superconductivity induced by surface functionalization.[25] Motivated by reports on superconductivity, we investigate the impact of functionalization on the superconducting properties of MXene, vanadium carbide (V_2C), which is intrinsically non-superconducting.[20]

In this work, we investigate the structural, electronic, vibrational, and superconducting properties of V_2C functionalized with (i) hydrogen, (ii) fluorine, and (iii) mixed hydrogen–fluorine, using density functional theory. The stability of these monolayers is confirmed by Born's mechanical stability criteria and the absence of imaginary frequencies in the phonon dispersion spectra. We also examine pristine V_2C MXene, which is non-superconducting, consistent with previous reports.[20] Upon functionalization, a significant enhancement in the electron–phonon coupling (EPC) constant is observed. Among the cases studied, mixed-functionalized V_2C exhibits the highest EPC constant, corresponding to a superconducting transition temperature of 7 K. These findings highlight mixed functionalization as a promising strategy for inducing superconductivity in MXenes. To further explore this concept, we extend our study to Nb_2C and observe an enhancement in its superconducting parameters.

2. Computational details

Theoretical calculations have been performed using the density functional theory (DFT) framework as implemented in the QUANTUM ESPRESSO package.[26] The norm-conserving Pseudo Dojo pseudopotentials of the Perdew–Burke–Ernzerhof (PBE) type have been employed.[27] The generalized gradient approximation of the Perdew–Burke–Ernzerhof type[28] is used for the exchange–correlation functional. For all the calculations, convergence criteria are set to 1.0×10^{-4} Ry Å^{-1} for forces and 1.0×10^{-5} Ry for energy. In order to avoid coupling between periodic images, we incorporated a vacuum space of around 20 Å along the *z*-axis in the structural models. The kinetic-energy cutoff for the wavefunctions is set to 100 Ry. A *k*-mesh of $36 \times 36 \times 1$ and a Methfessel–Paxton smearing with a width of 0.01 Ry are adopted for the structures. The elastic constants of pristine and functionalized V_2C are calculated with the help of Thermo pw code.[29] The phonon dispersion and electron–phonon coupling (EPC) calculations are performed by density functional perturbation theory (DFPT)[30] using a *q*-mesh of $6 \times 6 \times 1$. Using the density of states at the Fermi level (N_F), the matrix elements of the electron–phonon interaction ($g^{\nu}_{\mathbf{k},\mathbf{k}+\mathbf{q}}$), and the phonon ($\omega^{\nu}_{\mathbf{q}}$) and electronic ($\varepsilon_{\mathbf{k}}$) band structures obtained from our *ab initio* calculations, we computed the Eliashberg spectral function,[31]

$$\alpha^2F(\omega) = \frac{1}{N_F}\sum_{\nu,\mathbf{k},\mathbf{q}}\left|g^{\nu}_{\mathbf{k},\mathbf{k}+\mathbf{q}}\right|^2\delta(\omega-\omega^{\nu}_{\mathbf{q}})\delta(\varepsilon_{\mathbf{k}})\delta(\varepsilon_{\mathbf{k}+\mathbf{q}}), \quad (1)$$

for the different MXenes. The corresponding electron–phonon coupling (EPC) constant, λ, is obtained from;[32,33]

$$\lambda = 2\int_0^{\infty}\frac{\alpha^2F(\omega)}{\omega}\mathrm{d}\omega. \quad (2)$$

The superconducting transition temperature (T_c) is then estimated using the Allen–Dynes modified McMillan equation:[34]

$$T_c = \frac{\omega_{\log}}{1.2}\exp\left[-\frac{1.04(1+\lambda)}{\lambda-\mu^*(1+0.62\lambda)}\right], \quad (3)$$

where $\omega_{\log}$ is the logarithmically averaged phonon frequency, and μ^* represents the Coulomb pseudopotential, set to 0.1 in this study.

3. Results and discussion

3.1. Structural properties and stability analysis

Pristine V_2C crystallizes in the *P*3*m*1 space group, similar to the 1T-MoS_2 structure.[35] As shown in Fig. 1(a), V and C atoms in pristine V_2C are arranged in a triple-layer configuration along the hexagonal *c*-axis, with a C layer sandwiched between two V layers. The optimized lattice constant, *a*, is 2.891 Å, and the layer thickness *d* (defined by the V–V distance) is 2.174 Å, which is consistent with previously reported values.[36] Two types of hollow configurations are present on the surfaces: site A, located directly above or below the V atoms, and site B, located directly above or below the C atoms (Fig. 1(a)). Full surface adsorption is known to be energetically more favorable than partial adsorption.[37] The AA – adsorption configuration is also known to be the most stable for most MXenes.[21,24,36,38] We verified this by examining the relative stability of different adsorption configurations (see Table S1 in the ESI†), and found that the AA – adsorption configuration is indeed the most energetically favorable.

In this study, we consider V_2CX_2 structures (X = H, F, or mixed H and F) functionalized at the AA – adsorption configurations of V_2C. The optimized crystal structures of V_2CH_2, V_2CF_2, and V_2CFH are shown in Fig. 1(b)–(d), respectively, with structural parameters summarized in Table 1. Relative to pristine V_2C, hydrogen functionalization leads to an in-plane contraction, reducing the lattice constant from 2.891 Å to 2.874 Å

 This journal is © the Owner Societies 2025

Open Access Article. Published on 25 April 2025. Downloaded on 2/15/2026 1:18:58 AM.
This article is licensed under a Creative Commons Attribution-NonCommercial 3.0 Unported Licence.

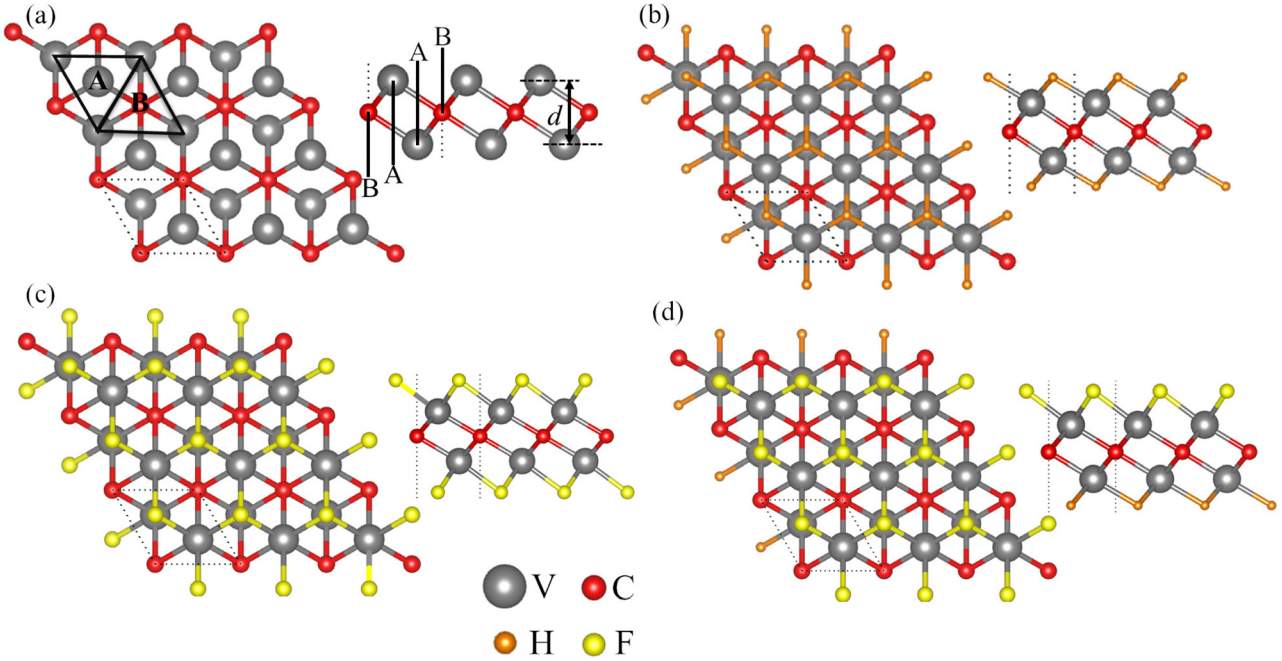

Fig. 1 Top and side view of (a) V_2C, (b) V_2CH_2, (c) V_2CF_2, and (d) V_2CFH. Here grey, red, orange, and yellow balls represent vanadium (V), carbon (C), hydrogen (H), and fluorine (F) atoms, respectively. In (a), A and B indicate the two types of hollow sites and *d* is the layer thickness.

Table 1 The calculated structural parameters and elastic constants for pristine and functionalized V_2C, wherein *a* and *d* denote the lattice constant and thickness of the compounds, and X is the functional group

	a (Å)	V–C (Å)	V–X (Å)	*d* (Å)	C_{11} (N m^{-1})	C_{12} (N m^{-1})	C_{22} (N m^{-1})	C_{66} (N m^{-1})
V_2C	2.891	1.99	—	2.174	153.376	69.620	153.376	41.878
V_2CH_2	2.874	2.00	1.93	4.213	191.554	13.917	191.554	88.818
V_2CF_2	2.986	2.00	2.14	4.595	173.812	72.167	173.812	50.822
V_2CFH	2.956	1.99	1.98, 2.14	4.371	190.221	56.902	190.221	66.659

due to the shorter V–H bond (1.93 Å). In contrast, fluorine functionalization induces in-plane expansion, increasing the lattice constant to 2.986 Å because of the longer V–F bond (2.14 Å). The structural parameters for V_2CF_2 agree well with previous reports.[36] For the mixed-functionalized V_2C, the lattice constant increases to 2.956 Å, the V–V distance decreases to 2.067 Å, and the layer thickness expands to 4.371 Å, reflecting the combined influence of H and F. The V–C bond remains at 1.99 Å, indicating a balance between the two functional groups (Table 1).

To evaluate the mechanical stability of these compounds under external load, we calculated their elastic constants. The Born mechanical stability criteria[39] for 2D hexagonal crystals require $C_{11} > 0$, $C_{66} > 0$ (with $2C_{66} = C_{11} - C_{12}$), and $C_{11} > C_{12}$. All the functionalized compounds V_2CX_2 (X = H, F, or mixed H and F) meet these criteria (see Table 1), suggesting that they may be synthesized under suitable experimental conditions. Notably, the elastic constants of these materials fall within the range observed for other 2D MXenes[40] but are lower than those of graphene,[41] indicating that they are less stiff and more flexible compared to graphene.

3.2. Electronic and vibrational properties

We calculated the band structure of pristine and functionalized V_2C using DFT to investigate their electronic properties. The projected band structures are plotted along the high-symmetry path Γ–M–K–Γ in the left panel of Fig. 2 and 3, with the corresponding projected density of states (PDOS) shown in the rightmost panels. The band crossings at the Fermi level indicate the metallic behavior of these materials, though variations in the electronic band structures are observed depending on the functional groups.

In pristine V_2C, the V-d_{z^2}, V-d_{zx}, and V-d_{xy} orbitals predominantly contribute to the bands near the Fermi level (Fig. 2(a)). In contrast, for V_2CH_2, the dominant contributions arise from V-d_{z^2}, V-$d_{x^2-y^2}$, and V-d_{zy} orbitals (Fig. 2(b)), while in V_2CF_2, the V-d_{z^2} and V-$d_{x^2-y^2}$ orbitals contribute primarily (Fig. 2(c)). Notably, a Dirac cone is observed above the Fermi level at approximately 0.8 eV at the K-point in V_2CH_2 (Fig. 2(b)), whereas in V_2CF_2, a Dirac cone appears around 0.3 eV below the Fermi level at the K-point (Fig. 2(c)), highlighting the potential of these materials for Dirac-physics-based applications. For the

Open Access Article. Published on 25 April 2025. Downloaded on 2/15/2026 1:18:58 AM.
This article is licensed under a Creative Commons Attribution-NonCommercial 3.0 Unported Licence.

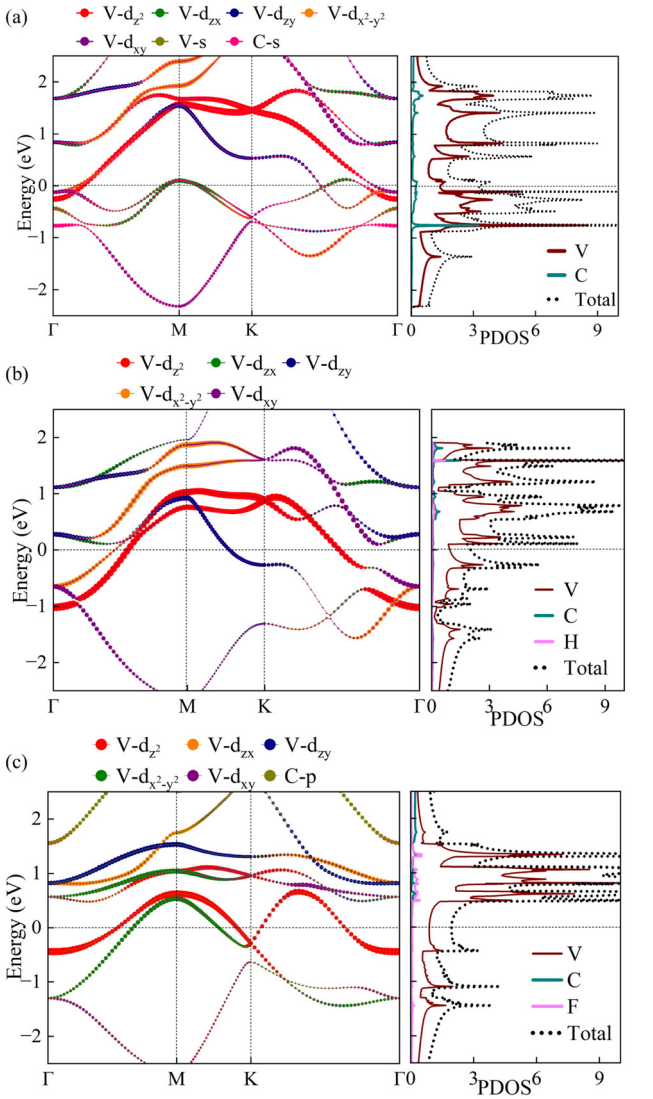

Fig. 2 Projected electronic band structure and projected density of states of (a) V_2C, (b) V_2CH_2, and (c) V_2CF_2.

mixed-functionalized V_2C (V_2CFH), the V-d_{z^2} and V-$d_{x^2-y^2}$ orbitals (Fig. 3) predominantly contribute at the Fermi level. The dominance of the V-d orbitals in all compounds is further confirmed by the PDOS plots, where only minor contributions from carbon and the functional groups are observed (rightmost panels of Fig. 2 and 3).

The phonon dispersion of pristine and functionalized V_2C is calculated using density functional perturbation theory (DFPT). The absence of imaginary frequencies in the phonon spectra indicates the dynamical stability of all compounds (Fig. 4–6).

The atom-resolved phonon dispersion is shown in the left panels, while the phonon density of states is presented in the rightmost panels. For V_2C, the phononic bands corresponding to constituent atoms are well-separated: the low-frequency phonon modes (up to 400 cm^{-1}) are primarily associated with V atom vibrations, while the high-frequency modes originate from C atom vibrations. These two sets of modes are separated by a phonon band gap of 254 cm^{-1} (31.491 meV) (Fig. 4(a)–(c)). Upon functionalization, this phononic band gap undergoes modifications.

In the case of hydrogen functionalization, additional high-frequency phonon modes emerge, leading to three distinct frequency regions in the phonon spectra: (i) low-frequency modes (up to 350 cm^{-1}), primarily dominated by V atom vibrations. (ii) Intermediate-frequency modes (650 cm^{-1} to 730 cm^{-1}), dominated by C atom vibrations. (iii) High-frequency modes (above 900 cm^{-1}), originating from H atom vibrations. This results in two phononic gaps of 315 cm^{-1} and 198 cm^{-1}, respectively (Fig. 5(a)–(d)).

Similarly, fluorine functionalization predominately leads to three frequency regions: (i) low-frequency phononic bands (up to 500 cm^{-1}), arising from both V and F contributions. (ii) Intermediate-frequency modes dominated by C vibrations. (iii) High-frequency modes, also dominated by C vibrations. The functionalization introduces a phononic gap of 134 cm^{-1} between the first and second regions and another gap of 99 cm^{-1} between the second and third regions (Fig. 5(f)–(i)).

For mixed functionalization with hydrogen and fluorine (V_2CFH), the phonon spectrum exhibits four distinct regions: (i) a low-frequency region (up to 500 cm^{-1}) with contributions from both V and F atoms. (ii) Two intermediate-frequency regions: 619 cm^{-1} to 654 cm^{-1} and 724 cm^{-1} to 768 cm^{-1}, dominated by C vibrations. (iii) Two high-frequency regions: 850 cm^{-1} to 914 cm^{-1} and 996 cm^{-1} to 1058 cm^{-1}, associated with H vibrations (Fig. 6(a)–(f)). V_2CFH features four phononic gaps: one large gap of 120 cm^{-1} and three smaller gaps of 74 cm^{-1}, 85 cm^{-1}, and 82 cm^{-1}. Notably, in both fluorine-functionalized (V_2CF_2) and mixed-functionalized (V_2CFH) cases, phonon softening occurs in the V-based ZA mode, particularly near the M point and along the K–Γ direction (Fig. 5(f) and 6(a)). In summary, functionalization modifies the phonon spectrum by introducing additional modes at higher frequencies and inducing phonon softening in the lower-frequency region. These changes may influence electron–phonon interactions and potentially affect superconducting properties.

3.3. Induced superconductivity in V_2C *via* functionalization

To investigate the superconducting properties of pristine and functionalized V_2C, we calculated their Eliashberg spectral function and electron–phonon coupling (EPC) constant from our DFPT results. We obtained a weak EPC constant of 0.28 for pristine V_2C (Fig. 4(d)), corresponding to a superconducting transition temperature (T_c) of 0.08 K, which is in agreement with earlier theoretical reports.[20] The EPC constant increases from 0.28 to 0.33 upon hydrogen functionalization of V_2C, corresponding to an increased superconducting transition temperature of T_c = 1.53 K (Fig. 5(e) and Table 2).

Up to the intermediate region, the EPC constant of V_2CH_2 remains comparable to that of pristine V_2C (0.28), as the phonon modes are predominantly associated with vanadium and carbon vibrations. However, due to the lighter mass of hydrogen, high-frequency phonon modes are introduced, providing additional EPC channels and enhancing the EPC

This journal is © the Owner Societies 2025

Open Access Article. Published on 25 April 2025. Downloaded on 2/15/2026 1:18:58 AM.
This article is licensed under a Creative Commons Attribution-NonCommercial 3.0 Unported Licence.

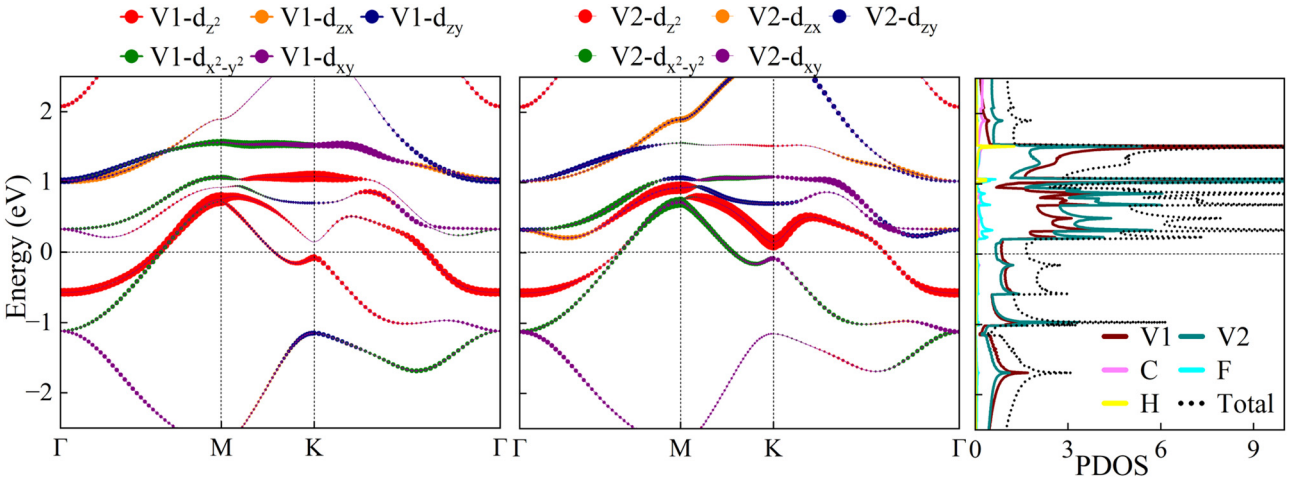

Fig. 3 Projected electronic band structure and projected density of states of V_2CFH.

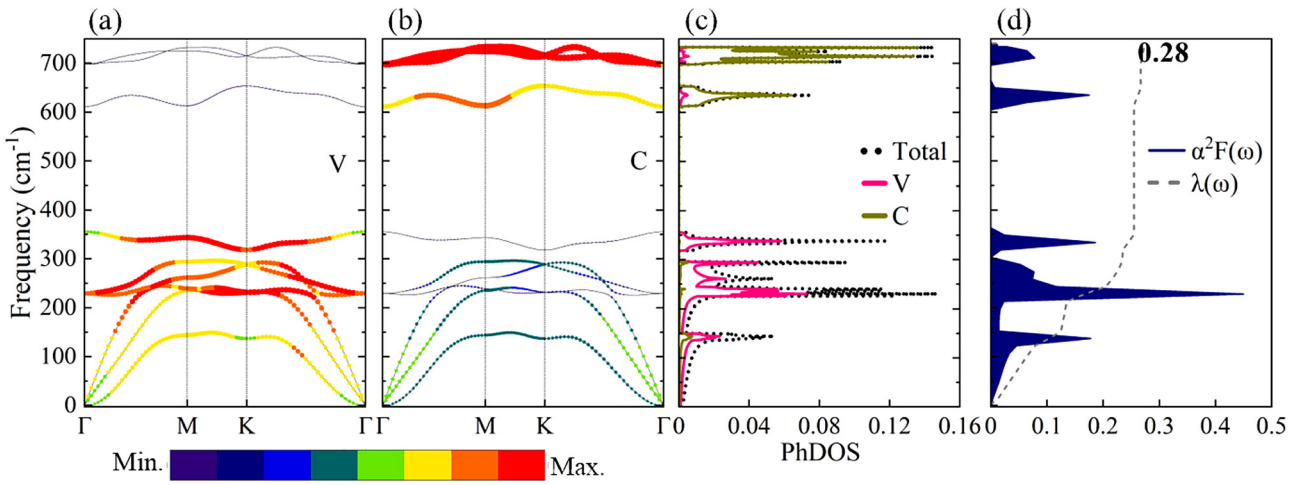

Fig. 4 (a) and (b) Phonon dispersion color-coded with atoms' contributions, (c) projected phonon density of states, and (d) Eliashberg spectral function (solid blue region) and EPC constant (dotted grey line) of V_2C.

constant to 0.33. It is worth noting that the T_c enhancement in V_2C is lower than that reported for other hydrogenated MXenes (Mo_2CH_2, Mo_2NH_2), likely due to the presence of phonon softening in those cases.[24] Upon fluorine functionalization, the EPC constant for V_2CF_2 increases to 0.55 (Fig. 5(j)), leading to a higher superconducting transition temperature (T_c) of 4.5 K. The enhancement in λ arises from two key factors: (i) the softening of the ZA phonon mode, which increases λ due to its frequency dependence (see Section 2), and (ii) the increased spectral weight in the low-frequency region (up to 500 cm^{-1}). The Eliashberg spectral function shows that this low-frequency region, dominated by vanadium and fluorine vibrations, contributes 94% (0.52 out of 0.55) to the total EPC constant. Compared to pristine V_2C and V_2CH_2, fluorine functionalization introduces additional phonon modes in the low-frequency region that couple with vanadium vibrations, playing a dominant role in enhancing the EPC constant and increasing T_c (Fig. 5(j) and Table 2). Upon mixed functionalization with hydrogen and fluorine, the EPC constant further increases to $\sim$ 0.6 (Fig. 6(g)), corresponding to a T_c of 7 K. The enhancement in superconductivity arises from the synergistic effect of fluorine-induced softening of the ZA phonon mode in the low-frequency region and the introduction of high-frequency phonon modes by hydrogen, which creates additional EPC channels. This study suggests that multi-element functionalization of MXenes could be a promising strategy for enhancing superconductivity. Further experimental and theoretical investigations are required to explore this effect in other MXene materials.

3.4. Inducing superconductivity in Nb_2C *via* mixed functionalization

We further extended our investigation of mixed functionalization to Nb_2C, a material previously reported to be non-superconducting both theoretically and experimentally.[19,20] As discussed above, AA – adsorption configurations are the most favorable for MXenes; hence, we consider the AA – adsorption

Open Access Article. Published on 25 April 2025. Downloaded on 2/15/2026 1:18:58 AM.
This article is licensed under a Creative Commons Attribution-NonCommercial 3.0 Unported Licence.

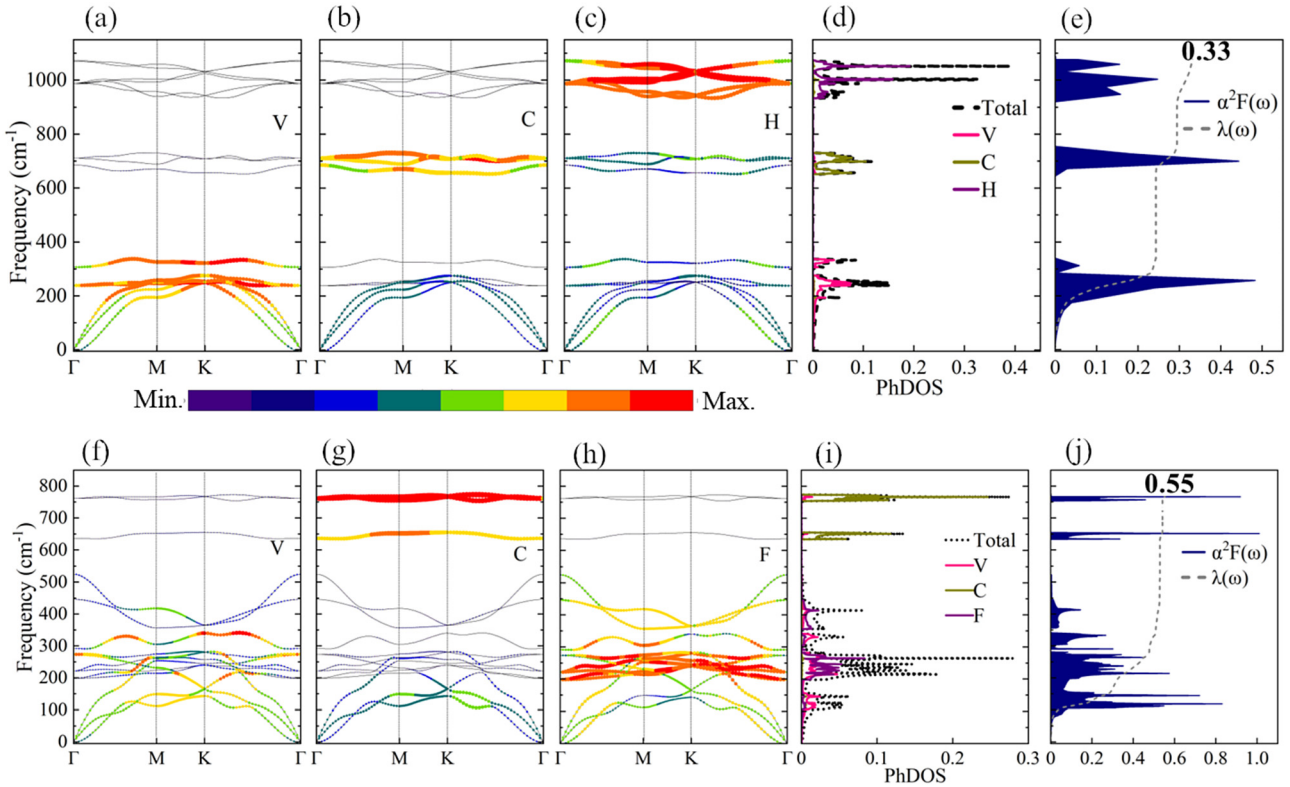

Fig. 5 Phonon dispersion color-coded with atoms' contributions and projected phonon density of states, and Eliashberg spectral function (solid blue region) and EPC constant (dotted grey line) of (a)–(e) V_2CH_2, and (f)–(j) V_2CF_2.

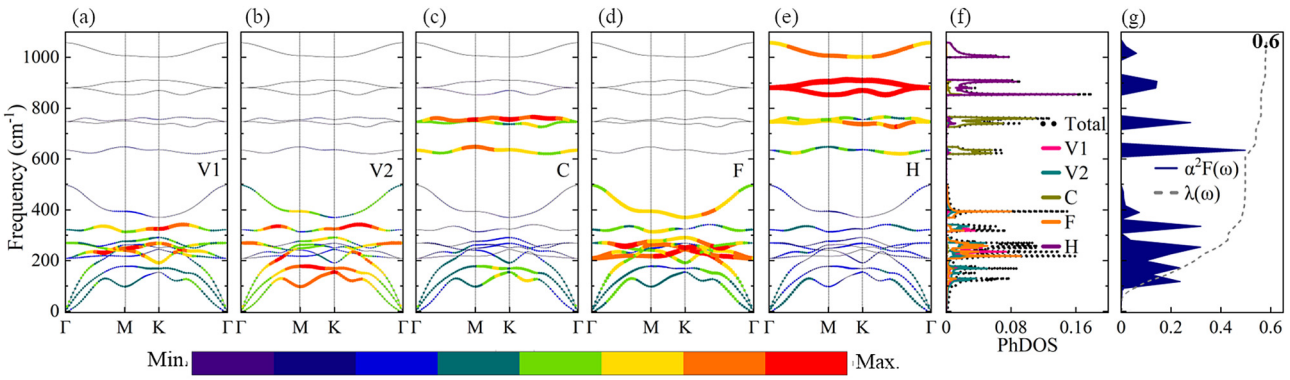

Fig. 6 (a)–(e) Phonon dispersion color-coded with atoms' contributions, (f) projected phonon density of states, and (g) Eliashberg spectral function (solid blue region) and EPC constant (dotted grey line) of V_2CFH.

configuration for mixed functionalization of Nb_2C with fluorine and hydrogen. The calculated lattice constant of Nb_2CFH is 3.193 Å, and the electronic band structure indicates metallic behavior (ESI† Fig. S1). The density of states at the Fermi level is 1.07 states per eV (Fig. S1, ESI†). We then calculated the phonon dispersion of Nb_2CFH to assess its stability. The absence of imaginary frequencies confirms its dynamical stability (Fig. 7(a)). Finally, the Eliashberg spectral function was computed to evaluate the electron–phonon coupling, revealing an enhanced EPC constant of 0.74 (Fig. 7(b)), corresponding to a T_c of 9.2 K (Table 2). The observed enhancement in EPC constant and T_c suggests a synergistic effect of fluorine and hydrogen vibrations, surpassing the EPC constant achieved in other single-atom functionalized Nb_2C systems such as Nb_2CH_2, Nb_2CBr_2, Nb_2CS_2, and Nb_2CCl_2, and approaches the highest reported T_c in Nb_2CO_2 (12 K).[21,38] These findings highlight the potential of mixed functionalization as an effective strategy for inducing and enhancing superconductivity in MXenes, offering a promising approach for tuning their superconducting properties.

 This journal is © the Owner Societies 2025

Open Access Article. Published on 25 April 2025. Downloaded on 2/15/2026 1:18:58 AM. This article is licensed under a Creative Commons Attribution-NonCommercial 3.0 Unported Licence.

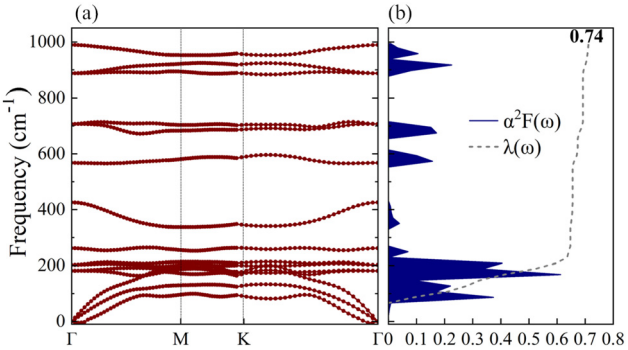

Fig. 7 (a) Phonon dispersion and (b) Eliashberg spectral function with EPC constant of Nb_2CFH.

Table 2 The average electron–phonon coupling constant λ and the estimated superconducting transition temperature T_c (K) for V_2C, V_2CH_2, V_2CF_2, and V_2CFH

	λ	T_c (K)
V_2C	0.28	0.08
V_2CH_2	0.33	1.53
V_2CF_2	0.55	4.5
V_2CFH	0.6	7.0
Nb_2CFH	0.74	9.2

4. Conclusions

We investigate the electronic structure, vibrational properties, and electron–phonon coupling (EPC) in V_2C-based MXenes, including pristine V_2C and functionalized V_2CX_2 (X = H, F, or mixed H–F functionalization). While pristine V_2C exhibits negligible EPC, rendering it unsuitable as a phonon-mediated superconductor, functionalization significantly enhances the EPC constant and induces superconductivity. In the case of mixed functionalization, the EPC constant reaches λ = 0.6, corresponding to a superconducting transition temperature (T_c) of 7 K, attributed to the synergistic vibrations of fluorine and hydrogen and the softening of the ZA phonon mode. Extending our study to another non-superconducting MXene, Nb_2C, we find that mixed functionalization further enhances the EPC constant to 0.74, resulting in a T_c of 9.2 K—higher than previously reported values for functionalized Nb_2C, including Nb_2CH_2, Nb_2CCl_2, Nb_2CS_2, and Nb_2CBr_2. These findings highlight the potential of mixed functionalization in MXenes for inducing superconductivity, offering promising avenues for designing high-performance two-dimensional superconductors.

Author contributions

Prarena Jamwal: conceptualization, methodology, data curation, investigation, formal analysis, visualization, validation, writing – original draft, writing – reviewing & editing. Rajeev Ahuja: writing – reviewing. Rakesh Kumar: supervision, writing – reviewing.

Data availability

The data supporting this study were obtained from first-principles density functional theory (DFT) calculations. All relevant computational details and results are provided in the manuscript and ESI.† Additional data can be made available upon request.

Conflicts of interest

There are no conflicts to declare.

Acknowledgements

P. J. acknowledges the National Supercomputing Mission (NSM) for providing computing resources of 'PARAM SMRITI' at NABI, Mohali, which is implemented by C-DAC and supported by the Ministry of Electronics and Information Technology (MeitY) and Department of Science and Technology (DST), Government of India. R. K. would like to acknowledge MeiTY (approval no. Y-20/8/2024 R&D-E) for the support.

Notes and references

1 M. Naguib, V. N. Mochalin, M. W. Barsoum and Y. Gogotsi, *Adv. Mater.*, 2014, **26**, 992–1005.
2 A. VahidMohammadi, J. Rosen and Y. Gogotsi, *Science*, 2021, **372**, eabf1581.
3 M. Narayanasamy, S. Zaman and C. M. Koo, *Mater. Today Energy*, 2023, **37**, 101405.
4 M. Hu, H. Zhang, T. Hu, B. Fan, X. Wang and Z. Li, *Chem. Soc. Rev.*, 2020, **49**, 6666–6693.
5 Á. Morales-García, F. Calle-Vallejo and F. Illas, *ACS Catal.*, 2020, **10**, 13487–13503.
6 D. H. Ho, Y. Y. Choi, S. B. Jo, J.-M. Myoung and J. H. Cho, *Adv. Mater.*, 2021, **33**, 2005846.
7 M. Khazaei, M. Arai, T. Sasaki, M. Estili and Y. Sakka, *Phys. Chem. Chem. Phys.*, 2014, **16**, 7841–7849.
8 I.-C. Lee, Y.-C. E. Li, J. L. Thomas, M.-H. Lee and H.-Y. Lin, *Mater. Horiz.*, 2024, **11**, 876–902.
9 S. Sun, C. Liao, A. M. Hafez, H. Zhu and S. Wu, *Chem. Eng. J.*, 2018, **338**, 27–45.
10 M. Naguib, M. W. Barsoum and Y. Gogotsi, *Adv. Mater.*, 2021, **33**, 2103393.
11 Y. Wei, P. Zhang, R. A. Soomro, Q. Zhu and B. Xu, *Adv. Mater.*, 2021, **33**, 2103148.
12 V. Kamysbayev, A. S. Filatov, H. Hu, X. Rui, F. Lagunas, D. Wang, R. F. Klie and D. V. Talapin, *Science*, 2020, **369**, 979–983.
13 B. Anasori, M. R. Lukatskaya and Y. Gogotsi, *Nat. Rev. Mater.*, 2017, **2**, 16098.
14 L. H. Karlsson, J. Birch, J. Halim, M. W. Barsoum and P. O. Å. Persson, *Nano Lett.*, 2015, **15**, 4955–4960.
15 K. J. Harris, M. Bugnet, M. Naguib, M. W. Barsoum and G. R. Goward, *J. Phys. Chem. C*, 2015, **119**, 13713–13720.

Open Access Article. Published on 25 April 2025. Downloaded on 2/15/2026 1:18:58 AM. This article is licensed under a Creative Commons Attribution-NonCommercial 3.0 Unported Licence.

16 J. Halim, K. M. Cook, M. Naguib, P. Eklund, Y. Gogotsi, J. Rosen and M. W. Barsoum, *Appl. Surf. Sci.*, 2016, **362**, 406–417.
17 H. Xia, L. Zhi, G. Feng, H. Cao, X. Xu, S. Zhang, J. Feng, C. Li, J. Li and P. Zhang, *J. Phys. Chem. Solids*, 2024, **193**, 112163.
18 M. Khazaei, A. Ranjbar, M. Arai, T. Sasaki and S. Yunoki, *J. Mater. Chem. C*, 2017, **5**, 2488–2503.
19 V. Kamysbayev, A. S. Filatov, H. Hu, X. Rui, F. Lagunas, D. Wang, R. F. Klie and D. V. Talapin, *Science*, 2020, **369**, 979–983.
20 J. Bekaert, C. Sevik and M. V. Milošević, *Nanoscale*, 2020, **12**, 17354–17361.
21 C. Sevik, J. Bekaert and M. V. Milošević, *Nanoscale*, 2023, **15**, 8792–8799.
22 K. Wang, H. Jin, H. Li, Z. Mao, L. Tang, D. Huang, J.-H. Liao and J. Zhang, *Surf. Interfaces*, 2022, **29**, 101711.
23 J.-J. Zhang and S. Dong, *J. Chem. Phys.*, 2017, **146**, 034705.
24 J. Bekaert, C. Sevik and M. V. Milošević, *Nanoscale*, 2022, **14**, 9918–9924.
25 M. Mozafari and M. Soroush, *Mater. Adv.*, 2021, **2**, 7277–7307.
26 P. Giannozzi, S. Baroni, N. Bonini, M. Calandra, R. Car, C. Cavazzoni, D. Ceresoli, G. L. Chiarotti, M. Cococcioni, I. Dabo, A. D. Corso, S. de Gironcoli, S. Fabris, G. Fratesi, R. Gebauer, U. Gerstmann, C. Gougoussis, A. Kokalj, M. Lazzeri, L. Martin-Samos, N. Marzari, F. Mauri, R. Mazzarello, S. Paolini, A. Pasquarello, L. Paulatto, C. Sbraccia, S. Scandolo, G. Sclauzero, A. P. Seitsonen, A. Smogunov, P. Umari and R. M. Wentzcovitch, *J. Phys.: Condens. Matter*, 2009, **21**, 395502.
27 M. van Setten, M. Giantomassi, E. Bousquet, M. Verstraete, D. Hamann, X. Gonze and G.-M. Rignanese, *Comput. Phys. Commun.*, 2018, **226**, 39–54.
28 J. P. Perdew, K. Burke and M. Ernzerhof, *Phys. Rev. Lett.*, 1996, **77**, 3865–3868.
29 A. Dal Corso, *J. Phys.: Condens. Matter*, 2016, **28**, 075401.
30 S. Baroni, S. de Gironcoli, A. Dal Corso and P. Giannozzi, *Rev. Mod. Phys.*, 2001, **73**, 515–562.
31 W. L. McMillan, *Phys. Rev.*, 1968, **167**, 331–344.
32 P. B. Allen and R. C. Dynes, *Phys. Rev. B*, 1975, **12**, 905–922.
33 P. B. Allen, *Phys. Rev. B*, 1972, **6**, 2577–2579.
34 R. Dynes, *Solid State Commun.*, 1972, **10**, 615–618.
35 Y. Linghu, N. Li, Y. Du and C. Wu, *Phys. Chem. Chem. Phys.*, 2019, **21**, 9391–9398.
36 A. Champagne, L. Shi, T. Ouisse, B. Hackens and J.-C. Charlier, *Phys. Rev. B*, 2018, **97**, 115439.
37 M. Khazaei, M. Arai, T. Sasaki, C.-Y. Chung, N. S. Venkataramanan, M. Estili, Y. Sakka and Y. Kawazoe, *Adv. Funct. Mater.*, 2013, **23**, 2185–2192.
38 Y. Yang and C. S. Ting, *J. Phys. D: Appl. Phys.*, 2020, **53**, 485301.
39 F. Mouhat and F. M. C.-X. Coudert, *Phys. Rev. B: Condens. Matter Mater. Phys.*, 2014, **90**, 224104.
40 U. Yorulmaz, A. Özden, N. K. Perkgöz, F. Ay and C. Sevik, *Nanotechnology*, 2016, **27**, 335702.
41 D. Çakr, F. M. Peeters and C. Sevik, *Appl. Phys. Lett.*, 2014, **104**, 203110.

 This journal is © the Owner Societies 2025